frontiers | Frontiers in Physics

TYPE Original Research
PUBLISHED 17 April 2023
DOI 10.3389/fphy.2023.1154159

OPEN ACCESS

EDITED BY
Jian Dong,
Central South University, China

REVIEWED BY
Nickolay Ivchenko,
Royal Institute of Technology, Sweden
Ningbo Wang,
Aerospace Information Research Institute (CAS), China
Wenwen Li,
Wuhan University, China

*CORRESPONDENCE
Feixue Wang,
fxwang@nudt.edu.cn

SPECIALTY SECTION
This article was submitted to Interdisciplinary Physics, a section of the journal Frontiers in Physics

RECEIVED 30 January 2023
ACCEPTED 28 March 2023
PUBLISHED 17 April 2023

CITATION
Li Z, Xiao W, Fan L, Lu Z and Wang F (2023), Impact of ambiguity resolution on phase center offsets and hardware delay estimation for BDS-3 inter-satellite links. *Front. Phys.* 11:1154159. doi: 10.3389/fphy.2023.1154159

Impact of ambiguity resolution on phase center offsets and hardware delay estimation for BDS-3 inter-satellite links

Zongnan Li[1], Wei Xiao[1], Lei Fan[2], Zukun Lu[1] and Feixue Wang[1]*

[1]College of Electronic Science, National University of Defense Technology, Changsha, China, [2]Scholol of Electronic Information Engineering, Beihang University, Beijing, China

The Chinese BeiDou navigation satellite system (BDS) has already completed its three phases and developed into a global navigation satellite system for open positioning, navigation, and timing services. The BDS-3 satellites feature the inter-satellite link (ISL). The ISL observation-related error model and ambiguity resolution for L-band observation are the crucial factors in precise data processing. In this study, we present for the first time the impact of ambiguity resolution on phase center offsets (PCOs) and hardware delay estimation of BDS-3 inter-satellite links. Two weeks' L-band observations from 99 globally distributed ground stations and Ka-band ISL observations are collected for experimental validation and analysis. First, network solutions with and without ISL observations are conducted to investigate the role of ISL observation in ambiguity resolution. Afterward, ISL observation-related errors, mainly PCOs and hardware delays, are estimated by processing L-band with ISL observations with and without ambiguity resolution to analyze the impact of ambiguity resolution on these two factors. Finally, orbit accuracy in the network solution is assessed to further validate the effectiveness of the estimated PCOs and hardware delays in our experiment. The result indicates that introducing the ISL can slightly improve the fixing rate compared to only L-band observations from 83.7% to 84.3%. Furthermore, ambiguity resolution has a positive influence on the stability of estimated PCOs and hardware delays in turn, although the root mean square (RMS) values basically remain unchanged. The standard deviation (STD) of the x-offset is reduced from 0.021 m to 0.012 m, a significant improvement of about 43%, and 0.022 m–0.016 m, with an improvement of about 27%, for the y-offset. There is a slight improvement of about 8% for z-offset. Similarly, around 10% improvement in the STD for hardware delays can be achieved while the RMS values almost stay the same except for C40. Orbit determination from network solutions shows high accuracy compared to the public products for the satellite with good geometry configuration, which further validates our estimates for ISL PCOs and hardware delays.

KEYWORDS

BDS-3, ambiguity resolution, PCO calibration, hardware delay, inter-satellite links, L-band

1 Introduction

The Chinese BeiDou navigation satellite system (BDS) has already completed its three phases and developed into a global navigation satellite system for open positioning, navigation, and timing services. The third phase, i.e., BDS-3, constellation consists of three geostationary Earth orbit (GEO) satellites, three inclined geosynchronous Earth orbit (IGSO) satellites, and 24 medium Earth orbit (MEO) satellites. The 24 BDS-3 MEO satellites are of the Walker 24/3/1 configuration with an altitude of 21528 km and an orbital inclination of 55°, placed in three orbital planes named A, B, and C with eight MEO satellites in each plane.

The BDS-3 satellites feature the inter-satellite link. It is a wireless link for communication and ranges between satellites or any other spacecraft. According to Wang et al. [1], the Ka-band-phased array antenna can scan the large space range of up to 70° with the antenna element and enable dynamic links between satellites. The ISL measurement is described by a dual one-way ranging model that follows a time division multiple access (TDMA) scheme. One satellite is linked with a different satellite according to a pre-designed timeslot scheduling; thus, the ISLs in the entire satellite network are set up. The timeslot scheduling defines how one satellite connects with the other satellite of the constellation through a polling mechanism. After transforming the dual one-way observations to the same epoch, clock-free and geometry-free observables can be obtained by the addition and subtraction of dual one-way observations, which is of great significance for a modern global navigation satellite system.

Until now, many studies on ISLs have been carried out, from the validation of the experimental satellite to those in-orbit operations. All the existing research can be divided into three categories, namely, observation quality analysis, autonomous navigation [2, 3], and the contribution to orbit determination and clock estimation through the joint use of L-band observations. As aspects of ISL observation quality, Tang et al. [4] and Zhou et al. [5] analyzed the characteristics of ISL measurement in detail using the geometry-free observables, whose noise is confirmed to be less than 10 cm. Xie and Wang [6–8] showed the visibility between the ISL and antennas of some BDS-3 satellites according to the dynamic satellite network topology. Many researchers have studied the autonomous navigation only with ISL observations, which is one of the original intentions of the ISLs. Initial results of centralized autonomous orbit determination of the new-generation BDS satellites with ISL measurements were shown in the study by Tang et al. [4]. Afterward, Guo et al. [9] proposed an on-board extended Kalman filter (EKF) method and conducted the orbit determination for BDS-3 satellites with a distributed mode. Ren et al. [10] compared the ISL orbit determination by batch processing and the EKF, and the orbit precision in the radial component for batch processing and the EKF is about 0.1 m and 0.3 m, respectively. In addition, the additional ISL ranging measurements can also improve the accuracy of orbit determination compared with only using the observations from ground stations, especially for GNSS whose ground stations are limited in regions such as the BDS. Wang et al. [8] and Ren et al. [10] presented model refinement and comparisons for the contribution of inter-satellite links to BDS-3 orbit determination. It showed that about a 40% improvement can be achieved for regional cases and 20% for global cases, after ISL data were used for precise orbit determination. Yang et al. [11, 12] and Xie et al. [6] analyzed the orbit and clock of BDS-3 using inter-satellite link observations, which showed its superiority to that of the L-band. Pan et al. [13] preliminarily evaluated the performance of ISL time synchronization by the relative clock offsets between two visible satellites computed by the BDS-3 ISLs.

Thanks to the detailed validation and analysis performed by these scholars, ISL data are currently used in daily data processing of the BDS-3 operational control system. Stable and reliable high-precision satellite orbit products are the prerequisites for the positioning services with high performances [14–16]. It should be noted that similar to L-band pseudo-range and carrier phase observations, the ISLs are also affected by the phase center offsets of the Ka-band-phased array antenna and hardware delay. As the *a priori* values of PCOs are gross estimates, it is necessary to calibrate them when the ISLs are combined with the L-band data. Meanwhile, in L-band satellite–ground precise orbit determination, the hardware biases are often absorbed in the estimated clock offsets, while for precise orbit determination, including the ISL clock-free observables, the hardware delay must be precisely calibrated. In precise data processing, strategies for dealing with these possible factors or errors caused by complex external observation environments will fall into two categories. One is the steady signal processing method on the front end [17–19], and the other is optimized observation processing strategies on the back end. Furthermore, ambiguity resolution for L-band observation [20–24] is the crucial factor in precise data processing, and various ambiguity resolution methods have been developed. However, current studies only involve PCOs or hardware delays for part of the satellites, and there is no exploration of the impact of ambiguity resolution on the estimation of two aspects for BDS-3 ISLs in network solutions using Ka-band and L-band observations. Thus, we present the calibration of PCOs and hardware delays for ISLs simultaneously and analyze the influence of ambiguity resolution on these two calibration values.

This paper is organized as follows: In Section 2, the basic models and methods are introduced. Section 3 describes the collected data and processing strategies. In Section 4, experiments are conducted. The performance of estimates of PCOs and hardware delays of ISL observations are analyzed, and the influence of ambiguity resolution on the estimates is discussed. Finally, the conclusions and discussion are provided.

2 Models and methods

This section describes the basic models and methods involved in our study. Starting from the original observations' equation of L-band and Ka-band ISL observables, along with the presented ambiguity resolution method used in our study, we derive the mathematical model for estimating ISL's PCOs and hardware delays simultaneously.

2.1 Basic observation equation

The L-band, i.e., pseudo-range and carrier phase observations, and Ka-band ISL observations follow different

structures. Herein, we express the L-band and Ka-band observation equations, respectively. Usually, to remove or weaken the influence of ionosphere delay, ionospheric-free combinations of the dual-frequency undifferenced code and carrier phase observations are used in precise orbit determination and positioning. The ionosphere-free (IF) combinations can be derived from the raw observations as

$$\begin{cases} L^s_{r,IF} = \rho^s_r + c\left(\delta\tilde{t}_r - \delta\tilde{t}^s\right) + T^s_r + \lambda^g_{IF}\left(b^g_{r,IF} - b^s_{,IF}\right) + \lambda^g_{IF}N^s_{r,IF} + \varepsilon_{L,IF} \\ P^s_{r,IF} = \rho^s_r + c\left(\delta\tilde{t}_r - \delta\tilde{t}^s\right) + T^s_r + c\left(d^g_{r,IF} - d^s_{,IF}\right) + \varepsilon_{P,IF} \end{cases}, \tag{1}$$

where r, s, and f are the indices of the receiver, satellite, and frequency, respectively; $L^s_{r,f}$ and $P^s_{r,f}$ are the phase and code observations with a unit of meter; ρ^s_r is the geometrical distance from the receiver to the satellite; $\delta\tilde{t}_r$ and $\delta\tilde{t}^s$ represent the receiver and satellite clock errors; c is the speed of light in vacuum; T^s_r is the troposphere delay, which can be corrected by a mathematical model to zenith troposphere delay (ZTD) of the receiver r; and $I^s_{r,f}$ denotes the ionospheric delay of the signal from the satellite to the receiver. λ^g_f and $N^s_{r,f}$ are the frequency-dependent wavelength and ambiguity of the phase observation, respectively. $b^g_{r,f}$ and b^s_f denote the hardware delay of phase observations from the receiver and satellite, respectively. Similarly, $d^g_{r,f}$ and d^s_f denote the ones of code observation. $\varepsilon_{L,f}$ and $\varepsilon_{P,f}$ are the measurement noise of phase and code observations.

It can be noticed that the hardware delay of code for the receiver and satellite is linearly dependent on the clock parameters, and the same is true for the hardware delay of phase with ambiguity parameters. Hence, in L-band-based observations, the hardware delay of code and phase for the receiver and satellite can be absorbed into the corresponding clock and ambiguity parameters.

The ISL ranging data are dual one-way range measurements following a time division multiple access structure. The forward and backward observations are at times whose difference is shorter than 3 s. Hence, it is necessary to transform the dual one-way measurements at the different times to a common epoch $\bar{t}$; that is,

$$\begin{cases} P_{AB}(\bar{t}) = P_{AB}(t_1) + \Delta P_{AB} = \rho_{AB}(\bar{t},\bar{t}) + c\cdot\left[dt_B(\bar{t}) - dt_A(\bar{t})\right] + c\left(\delta^{rec}_B + \delta^{send}_A\right) + \varepsilon_1 \\ P_{BA}(\bar{t}) = P_{BA}(t_2) + \Delta P_{BA} = \rho_{AB}(\bar{t},\bar{t}) + c\cdot\left[dt_A(\bar{t}) - dt_B(\bar{t})\right] + c\left(\delta^{rec}_A + \delta^{send}_B\right) + \varepsilon_2 \end{cases}, \tag{2}$$

where $P_{AB}(t_1)$ and $P_{BA}(t_2)$ are the forward and backward ISL observations at the receiver time. $P_{AB}(\bar{t})$ and $P_{BA}(\bar{t})$ denote the transformed observations at $\bar{t}$. ΔP_{AB} and ΔP_{BA} represent the correction differences of the satellite distance and clock biases between the observed epoch and the target epoch $\bar{t}$. $\rho_{AB}(\bar{t},\bar{t})$ is the instantaneous distance between two satellites. c is the velocity of the light in vacuum. $dt_A(\bar{t})$ and $dt_B(\bar{t})$ are clock biases of satellite A and satellite B,respectively, at the same time $\bar{t}$. Analogously, δ^{rec}_B, δ^{send}_A, δ^{rec}_A, and δ^{send}_B are the hardware delays. ε_1 and ε_2 represent the corresponding measurement delays.

The sum of $P_{AB}(\bar{t})$ and $P_{BA}(\bar{t})$ forms a clock-free observation and is used for the orbit determination, while the subtraction of $P_{AB}(\bar{t})$ and $P_{BA}(\bar{t})$ forms a geometry-free observables and is usually used for the satellite clock bias estimation. Without derivation, we directly present the common observation equation of ISL as follows:

$$\begin{cases} \dfrac{P_{AB}(\bar{t}) + P_{BA}(\bar{t})}{2} = \left|\vec{R}_B(\bar{t}) - \vec{R}_A(\bar{t})\right| + c\cdot\left(\bar{X}^A_{delay} + \bar{X}^B_{delay}\right) + \dfrac{\Delta\rho^{AB}_{cor} + \Delta\rho^{BA}_{cor}}{2} \\ \dfrac{P_{AB}(\bar{t}) - P_{BA}(\bar{t})}{2} = c\cdot\left[dt_B(\bar{t}) - dt_A(\bar{t})\right] + c\cdot\bar{\bar{X}}^A_{delay} - c\cdot\bar{\bar{X}}^B_{delay} + \dfrac{\Delta\rho^{AB}_{cor} - \Delta\rho^{BA}_{cor}}{2} \end{cases}, \tag{3}$$

where $\bar{X}^A_{delay}$ and $\bar{X}^B_{delay}$ indicate the satellite-specific hardware delays; $\Delta\rho^{AB}_{cor}$ and $\Delta\rho^{BA}_{cor}$ represent the geometry-related corrections such as priori PCOs, yaw attitude, relativistic effects, and noise. $\vec{R}_B$ and $\vec{R}_A$ are the vectors of two satellites. What needs to be emphasized is that here, PCOs are calibrated after corrections; thus, $\vec{R}_B$ and $\vec{R}_A$ contain the satellite positions and PCOs.

2.2 Virtual observation equation from ambiguity resolution

Carrier phase observation is widely applied in precise orbit determination and positioning thanks to the high precision of measurement at the level of centimeter to millimeter, provided that cycle slips and ambiguity are well dealt with. As is known, the ambiguity parameters are easy to lose their integer characteristic and are, thus, estimated as float because of the linear dependence on some other parameters, such as hardware delay and initial phase bias [20–24]. Recovering their integer characteristic can effectively improve the accuracy of parameter solutions, and many ambiguity resolution methods and methods have been developed [25–30]. In our study, the double-differenced ambiguity resolution methods described by Ge et al. [21] are adopted. It can be expressed as

$$\begin{cases} \Delta\nabla N_{IF} = \dfrac{f_1\cdot f_2}{f_1^2 - f_2^2}\Delta\overline{\nabla N}_{WL} + \dfrac{f_1}{f_1 + f_1}\Delta\nabla\bar{N}_{NL}, P = 10^8 \\ \Delta\nabla N_{IF} = N^s_{r1,IF} - N^s_{r2,IF} - N^{s_{ref}}_{r1,IF} + N^{s_{ref}}_{r2,IF} \end{cases}, \tag{4}$$

where $\Delta\overline{\nabla N}_{WL}$ and $\Delta\nabla\bar{N}_{NL}$ are recovered integer wide-lane and narrow-lane ambiguities, respectively; $N^s_{r1,IF}$, $N^s_{r2,IF}$, $N^{s_{ref}}_{r1,IF}$, and $N^{s_{ref}}_{r2,IF}$ denote the four-involved undifferenced float ambiguity solutions for receivers $r1$ and $r2$ and satellite s and s_{ref}. P is the weight of the virtual observation equation. If the wide-lane and narrow-lane ambiguities of double-differenced ambiguity are fixed to integer ones in sequence, then the fixed ambiguity of ionosphere-free combinations can be derived. It will be regarded as virtual observation equations processed together with the observation equations with a strong constraint. In this way, ambiguity resolution is achieved in network solutions using L-band and Ka-band data to estimate the PCOs and hardware delays of ISL observations.

2.3 Mathematical model for estimation

The previous equations, the basic observation equation for L-band and Ka-band measurements, and the virtual observation equation from ambiguity resolution are processed together in our study to calibrate the ISL's PCOs and hardware delays simultaneously in network solutions. To be consistent with the

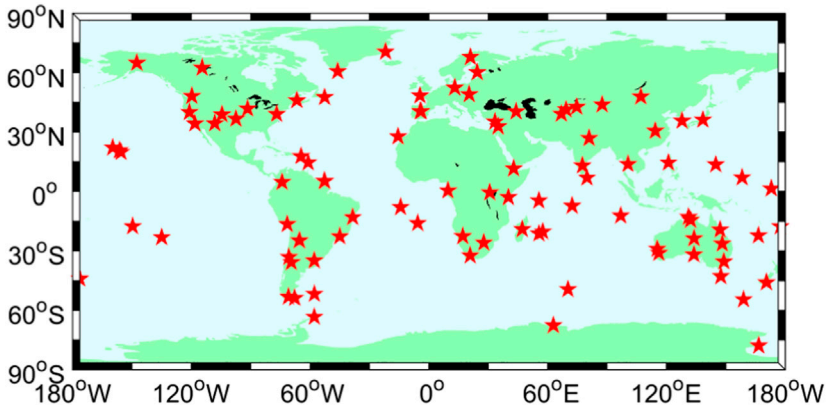

FIGURE 1
Distribution of 99 stations selected for calibration of PCOs and hardware delays for ISLs.

TABLE 1 Processing strategies, models, and estimated parameters.

Item		Contents
Observation	Data length	14 days from DOY 289 to DOY 302, 2020
	Observables	Undifferenced ionosphere-free code and phase combination
		ISLs
	Cut-off elevation	7°
	Processing arc	24 h
	Processing interval	30 s
	Weighting	Elevation-dependent, 1 for $E > 30°$, otherwise $2\sin(E)$
Processing models	PCO and PCV of the receiver	Igs_14.atx
	Tropospheric delay	Sasstamoinen model, mapping function GMF [31]
	DCB	P1-C1.DCB products published by CODE [32]
Dynamic models	N-body gravity	Sun, Moon and planets, physical attributes, and ephemeris: JPL DE405
	Geopotential	EGM 2008 model (12 × 12)
	Tidal forces	Solid tide, ocean tide, pole tide
		IERS Conversion 2010 [33]
	Solar radiation pressure	Priori Box-wing and 7-parameters ECOM-2 [34, 35]
	Earth-albedo radiation pressure	Model by Rodriguez-Solano et al [36]
	Relativistic effects	IERS Conversion 2010 [33]

orbit dynamics, we express the linearized observation equations in the earth-centered inertial (ECI) frame. By combining the code phase with ISL observation equations, we can get the mathematical model for the network solution; that is,

$$\begin{cases} \boldsymbol{L}_{sta} = \boldsymbol{G}\left(\boldsymbol{x}_s^0, \boldsymbol{x}_r, \boldsymbol{x}_{erp}, \boldsymbol{x}_0, t\right) + \varepsilon_{sta} \\ \boldsymbol{L}_{isl-s} = \boldsymbol{R}\left(\boldsymbol{x}_s^0, \boldsymbol{x}_0, \boldsymbol{x}_{pco}, \boldsymbol{x}_{bias}, t\right) + \varepsilon_{isl-s} \end{cases}, \tag{5}$$

where $\boldsymbol{L}_{sta}$ and $\boldsymbol{L}_{isl-s}$ are observations of the stations and inter-satellite links, respectively. $\boldsymbol{G}$ and $\boldsymbol{R}$ describe the functional model between the corresponding observations and estimated parameters. The estimated parameter $\boldsymbol{x}_s^0 = (\boldsymbol{r}_s^0, \dot{\boldsymbol{r}}_s^0, \boldsymbol{p}_s)$ denotes the orbit-related status parameters, where $\boldsymbol{r}_s^0$ and $\dot{\boldsymbol{r}}_s^0$ are the initial position vector and velocity of the BDS satellite, respectively. $\boldsymbol{p}_s$ expresses the dynamic-related parameters. $\boldsymbol{x}_r$ is the vector of the site coordinate. $\boldsymbol{x}_{erp}$ represents the vector of Earth rotation parameters. $\boldsymbol{x}_0$ denotes the other observation-related parameter, such as the clock of satellites and receivers, tropospheric delay, and ambiguity of phase. Usually, PCOs of the L-band have public products, and the bias of L-band observation can be absorbed into the clock of the satellite and

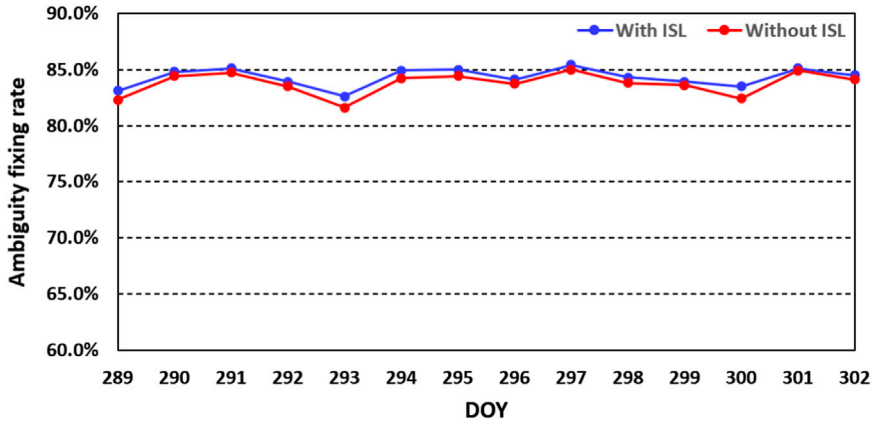

FIGURE 2
Daily fixing rate of ambiguity resolution with ISL observation (blue line) and without ISL observations (red line) during DOY 289-302, 2020.

TABLE 2 Statistical fixing rate with and without ISL observations.

	Without ISL (%)	With ISL (%)
Max	85.00	85.40
Min	81.60	82.60
Average	83.76	84.30

receiver. However, the ISL's PCOs and bias should be considered. Within the estimation, they are taken as constants, $\boldsymbol{x}_{pco}$ for the phase center offsets and x_{bias} for hardware delay; t expresses the current epoch; ε_{sta} and ε_{isl-s} are the observation noise for observations of stations and inter-satellite links, respectively. After linearization, we can get the error equation as

$$\begin{bmatrix} \boldsymbol{v}_r \\ \boldsymbol{v}_{isl-s} \end{bmatrix} = \begin{bmatrix} \frac{\partial \boldsymbol{G}}{\partial \boldsymbol{x}_s^0} & \frac{\partial \boldsymbol{G}}{\partial \boldsymbol{x}_r} & \frac{\partial \boldsymbol{G}}{\partial \boldsymbol{x}_{erp}} & \frac{\partial \boldsymbol{G}}{\partial \boldsymbol{x}_0} & \boldsymbol{0} & \boldsymbol{0} \\ \frac{\partial \boldsymbol{R}}{\partial \boldsymbol{x}_s^0} & \boldsymbol{0} & \boldsymbol{0} & \frac{\partial \boldsymbol{R}}{\partial \boldsymbol{x}_0} & \frac{\partial \boldsymbol{R}}{\partial \boldsymbol{x}_{pco}} & \frac{\partial \boldsymbol{R}}{\partial x_{bias}} \end{bmatrix} \cdot \begin{bmatrix} \delta \boldsymbol{x}_s^0 \\ \delta \boldsymbol{x}_r \\ \delta \boldsymbol{x}_{erp} \\ \delta \boldsymbol{x}_0 \\ \delta \boldsymbol{x}_{pco} \\ \delta x_{bias} \end{bmatrix} - \begin{bmatrix} \boldsymbol{l}_{sta} \\ \boldsymbol{l}_{isl-s} \end{bmatrix}, \tag{6}$$

where $\boldsymbol{v}_r, \boldsymbol{v}_{isl-s}$ and $\boldsymbol{l}_r, \boldsymbol{l}_{isl-s}$ are residual and observation minus calculation for L-band and ISL observation, respectively; $\frac{\partial \boldsymbol{G}}{\partial \boldsymbol{x}}, \frac{\partial \boldsymbol{R}}{\partial \boldsymbol{x}}$ represent the linearization coefficients; e.g., $\frac{\partial \boldsymbol{G}}{\partial \boldsymbol{x}_s^0}$ is the coefficient between $\boldsymbol{L}_{sta}$ and the estimated parameter $\boldsymbol{x}_s^0$. $\delta \boldsymbol{x}_s^0, \delta \boldsymbol{x}_r, \delta \boldsymbol{x}_{erp}, \delta \boldsymbol{x}_0, \delta \boldsymbol{x}_{pco}, \delta x_{bias}$, and the estimated variations for estimated parameters are compared to the initial value in linearization. Solving the previous equations using the least-squares method in the batch processing mode, we can get the initial estimates. Then, ambiguity resolutions start to fix the estimated float ambiguity to the integer ones and form virtual observations. Finally, virtual observation equations are added to the previous equations, and the same process is dealt with again. In this way, the estimated ISL's PCOs and hardware delays can be obtained through ambiguity resolution.

3 Data collection and strategy

The BDS-3 satellites have been put into operation for more than 2 years. As equipment continues to upgrade, more and more receivers provided by the International GNSS Service (IGS) can support BDS-3 observations. To validate the proposed algorithm and get stable results for all BDS-3 satellites, we collect ISL data from all BDS-3 satellites and select L-band data from 99 globally distributed stations. The detailed descriptions of BDS-3 ISL can be referred to in existing articles; here, we will not go into detail. All selected stations have the capacity to track the B1I and B3I signals of BDS-3 satellites for network solutions. The distribution of these stations is shown in Figure 1.

Specifically, 2 week data from DOY 289 to DOY 302, 2020, are used to generate the network solutions, including orbit-related parameters, the coordinate of receivers, the clock of satellite and receiver, zenith tropospheric delays, and ambiguities. Furthermore, the PCOs and hardware delays of Ka-band ISL observations are estimated. Table 1 summarizes the detailed models and estimated parameters.

All parameters are estimated using the batch processing method. Cycle slips are detected, and gross errors are removed before parameter estimation. The orbit-related status parameters, receiver coordinates, and ambiguities are estimated as constant parameters, while the clocks of the receivers and satellites and the zenith tropospheric wet delay are estimated as random parameters. Ambiguities estimated as float and integer ones are done, respectively.

4 Experiments and analysis

We first investigate the effectiveness of ambiguity resolution in network solutions with and without ISLs in terms of fixing rates. Then, the performance of estimated ISL's PCOs and hardware delays and the impact of ambiguity resolution on them are analyzed in detail. Finally, the orbit accuracy of satellites produced in the network solution is evaluated.

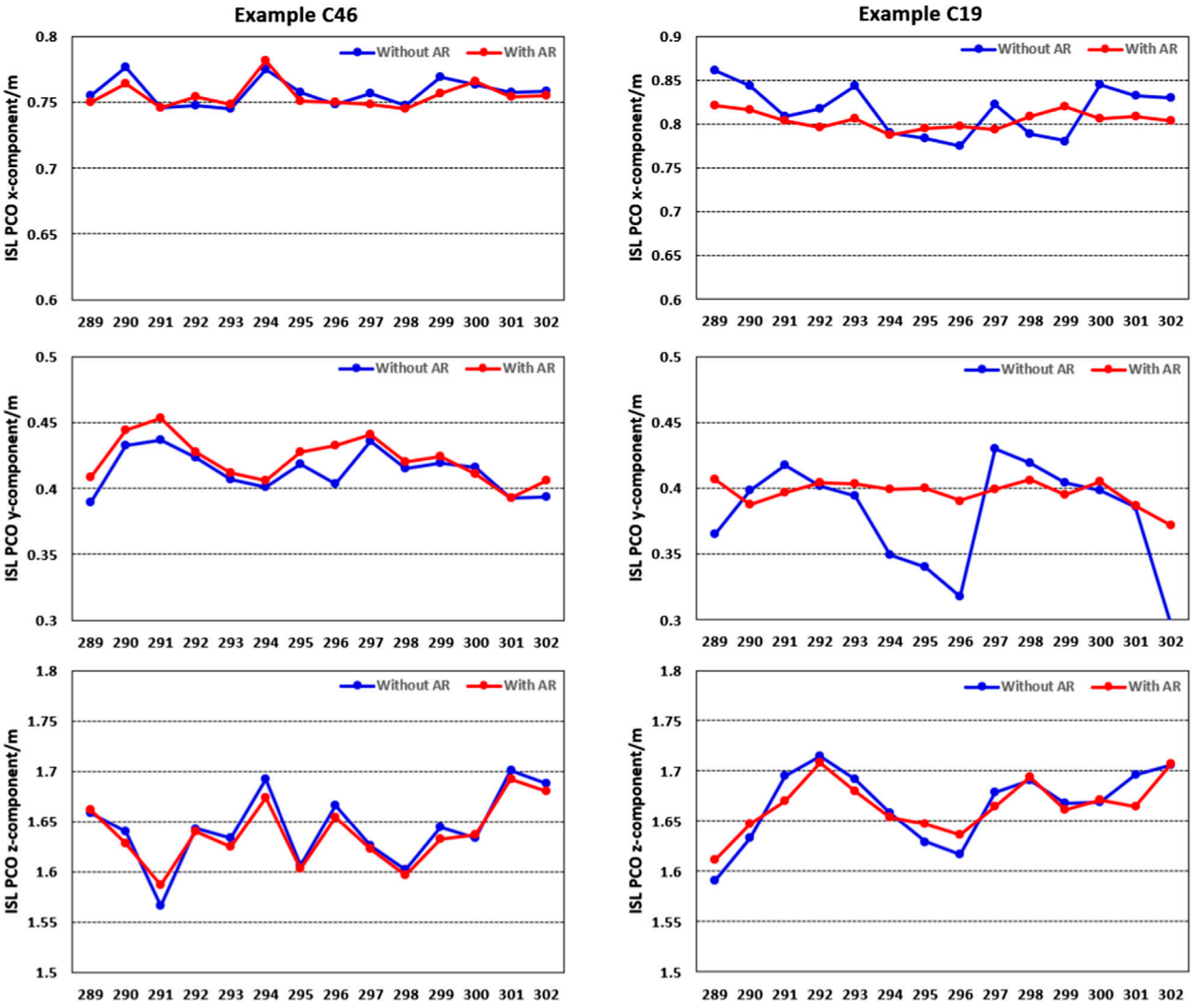

FIGURE 3
Daily estimated ISL PCOs in the x-component, y-component, and z-component with and without ambiguity resolution, respectively, for C46 and C19 during 14 days.

4.1 Fixing rate

As is known, ambiguity resolution can improve the accuracy of orbit determination and positioning for L-band observations. Furthermore, in this section, the contribution of introducing ISL observations processed together with L-band observations to ambiguity resolution is explored for the first time.

Two experimental schemes are designed, namely, L-band ambiguity resolution and L-band + Ka-band ambiguity resolution. Fixing rate is chosen as the indicator, which is the proportion of fixed double-differenced ambiguity to all double-differenced ambiguity. The statistical results are shown in Figure 2; Table.2.

We can see that, under the condition of a cautious empirical threshold for wide-lane deviation, narrow-lane deviation, and ratio as 0.25 cm, 0.2 cm, and 3, the statistical daily fixing rate keeps stable among different days at the level of about 83.5%. What is more notable is that there is a slight improvement in the fixing rate when ISL observations are introduced. The fixing rate increases up to about 84.5%. That is, ISL observations perform a positive influence on the ambiguity resolution for L-band observation in the network solutions. It can make contributions to the fixing rate with a proportion of about 1%. This may be due to the accuracy improvement of estimated parameters thanks to the stronger geometry characteristic. Therefore, this, in turn, inspires us to further investigate the impact of ambiguity resolution on the estimation of ISL-related errors, such as PCOs and hardware delays.

4.2 ISL PCOs

Usually, the GNSS orbit is computed with respect to the mass center of the satellite. However, the observation refers to the

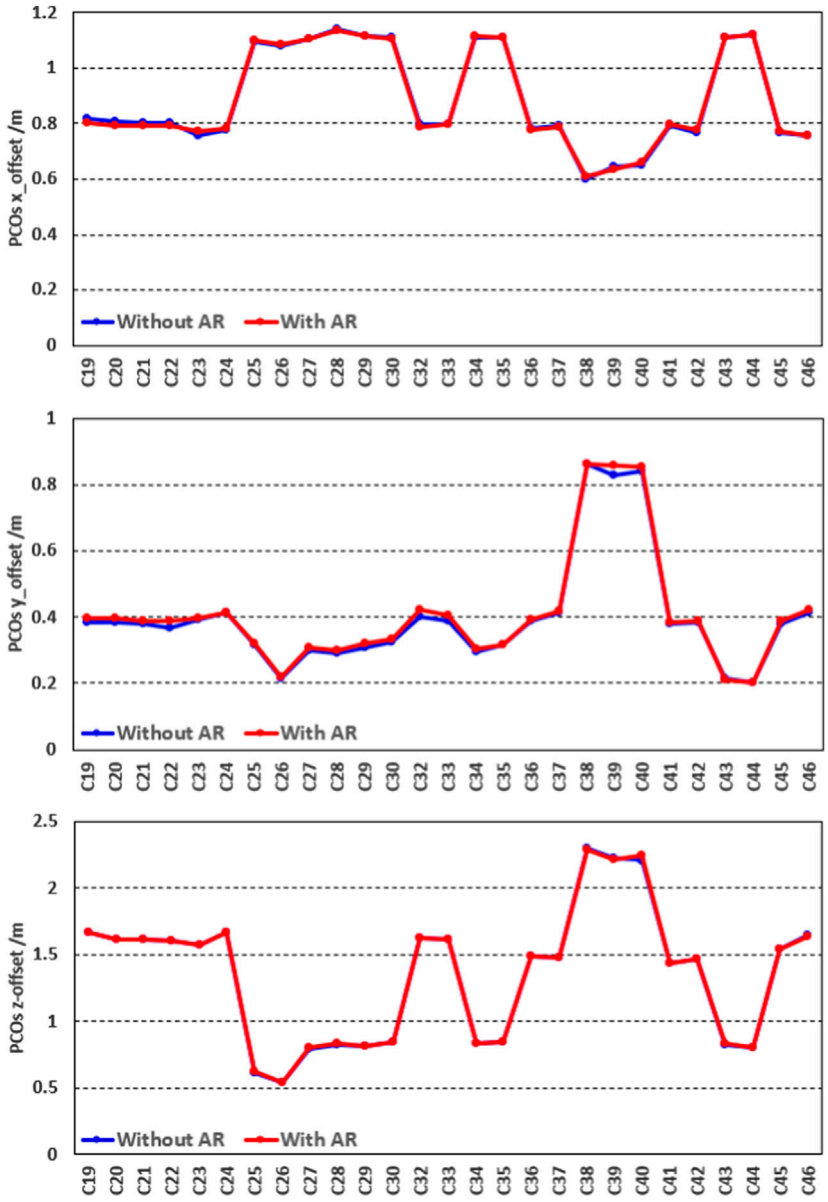

FIGURE 4
Statistical RMS values of PCOs in the x-component (upper panel), y-component (middle panel), and z-component (bottom panel) with ambiguity resolution (the red line) and without ambiguity resolution (the blue line), respectively, for all BDS-3 satellites during 14 days.

antenna's phase center. The offset between these two centers must be known. In fact, the offset is difficult to measure since the phase center is not a mechanical point but an electronic one. So, the calibration before injection will strictly not be an exact value, and calibration after in-orbit is necessary.

In our study, the ISL PCOs are regarded as constant over a 24 h arc. Through processing L-band and ISL observations together in network solutions, we obtain ISL PCOs for all BDS-3 satellites. Taking C46 as an example, the daily estimated values in the x-component, y-component, and z-component are presented in Figure 3 as follows.

As can be seen from the abovementioned figure, there is very good consistency in each component between different days. Considering the stability of daily estimates, we calculate the RMS and STD values of all results over 14 days for each satellite. The details are shown in Figures 4, 5, respectively.

As shown in Figure 4, the RMS of estimated ISL PCOs presents a slight difference in all three components between results with and without ambiguity resolution for almost satellites. The z-offsets show the best consistency for all satellites; x-offsets are the second, while a slight difference can be found in the y-offsets for some satellites. In addition, it is obvious that ISL PCOs of some satellites almost stay at the same level. By collecting the information on satellite and inter-satellite link payload manufacturers, shown in Table 3, we find the correlation. ISL PCOs of the satellites from the

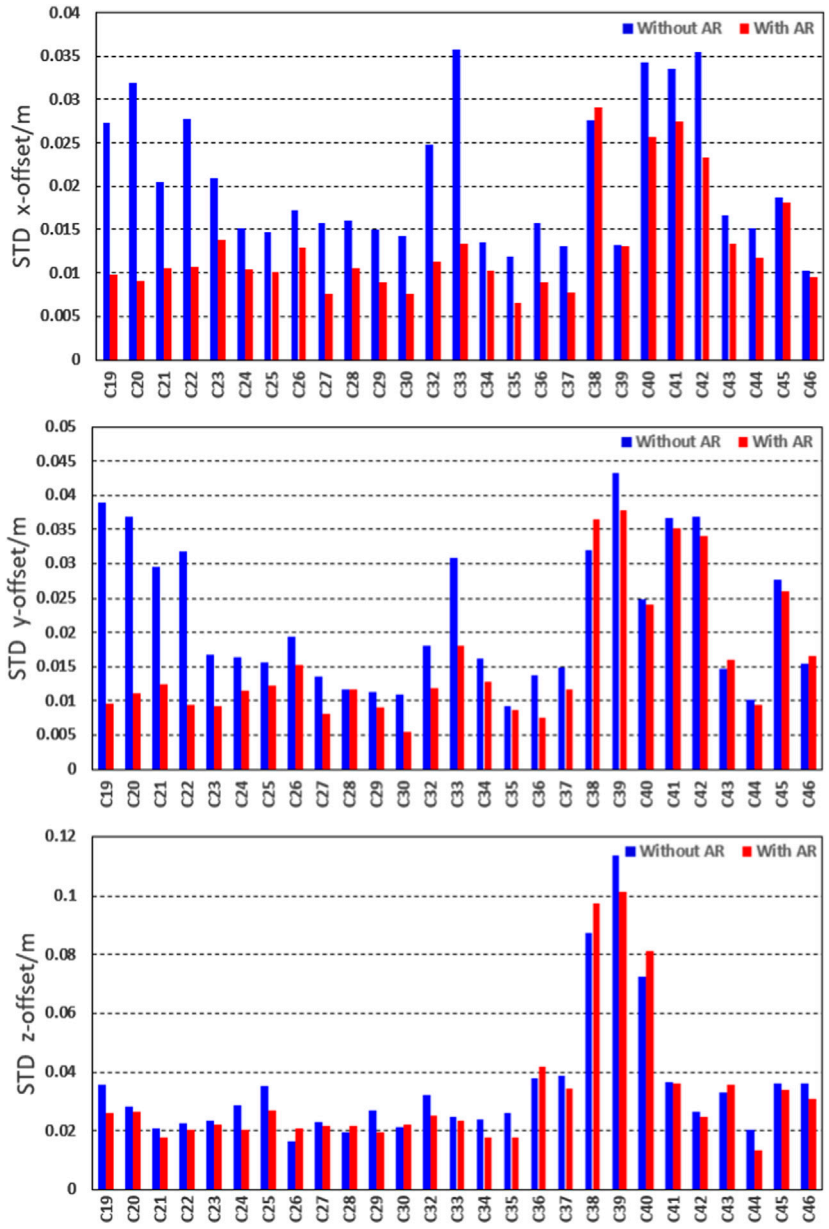

FIGURE 5
Statistical STD values of calibrated PCOs in the x-component (the upper panel), y-component (the middle panel), and z-component (the bottom panel) for all BDS-3 satellites without ambiguity resolution (the blue bars) and with ambiguity resolution (the red bars) during 14 days.

TABLE 3 Information about the manufacturer of satellite and inter-satellite link payload.

Satellite	Inter-satellite link payload	PRN
CAST	CASC1	C19–C22, C24, C33, C37–C42, C46–C61
	CASC2	C23, C32, C36, C45
SCEM	SCEM1	C27, C29, C39, C34, C35, C43, C44
	SCEM2	C25, C26
	SCEM3	C28

TABLE 4 Statistical STD values for the estimated ISL's PCOs.

Indictor	x-offset (m)		y-offset (m)		z-offset (m)	
	Float	Fix	Float	Fix	Float	Fix
Average	0.021	0.012	0.022	0.016	0.035	0.032
Max	0.036 (C33)	0.029 (C38)	0.043 (C39)	0.038 (C39)	0.113 (C39)	0.101 (C39)
Min	0.010 (C46)	0.006 (C35)	0.009 (C35)	0.005 (C30)	0.016 (C26)	0.013 (C44)

same manufacturer perform similar characteristics, except for the three IGSO satellites, i.e., C38–C40.

Then, we calculate the standard deviation for all satellites using daily estimations. The results are as follows in Figure 5.

From Figure 5, we can see that the STD of the estimated ISL PCOs with ambiguity resolution decreases obviously overall compared to the ones without ambiguity resolution. In other words, the stability of estimated ISL PCOs improves. To be more specific, different satellites show various improvements, and different components perform differently. Despite the ambiguity resolution, the z-offset stays almost the same for most satellites. Only a slight improvement can be found for C19, C24, C25, C29, C34, C35, and C39. Moreover, it is noteworthy that the STD of PCOs in z-offset estimation keeps around 0.02 m for almost all satellites except for three satellites in the IGSO, i.e., C38, C39, and C40, whose STD values reach up to around 0.08 m. For the x-offset and y-offset, obvious improvements can be seen for most satellites. We discover that the largest improvement occurs on C19, C20, C21, C22, and C33. After ambiguity resolution, the STD of PCOs estimation is about 0.012 m and 0.016 m for the x-offset and y-offset, respectively. The statistical average value and maximum and minimum STD values are shown in Table 4.

Based on the previous results, we can draw a preliminary conclusion that ambiguity resolution plays a positive role in the stability of the ISL PCO estimation. There is an obvious improvement for STD values by 43%, 27%, and 8% for the x-offset, y-offset and z-offset, respectively.

4.3 ISL hardware delay

Hardware delays always exist in navigation measurements. The most recognized hardware delay is the L-band pseudo-range bias associated with both the GNSS satellite and receiver. This hardware delay is often determined as the differential code bias (DCB), which is the differential hardware delay between two or more frequencies [30]. The DCB parameters are typically incorporated into the definition of the clock for the dual- or triple-frequency L-band code measurement. ISL measurement also suffers from the hardware delay. However, unlike the DCBs of the pseudo-range measurement, which are estimated in a relative sense, the ISL hardware delay is the absolute delay between the ISL measurement and the geometric distance.

We estimate the ISL hardware delay together with the previous ISL PCOs in the network solution. All strategies are the same as the ISL PCO calibration. Like the evaluation of PCOs, the RMS and STD of the estimated hardware delay with and without ambiguity resolution are also counted and analyzed. Figure 6 shows the absolute value of the hardware delay and its time series for C19, C37, and C46. It can be seen that the estimated hardware delays are stable for 2 weeks, and ambiguity resolution plays a positive role in the stability.

Considering the various ISL hardware delay magnitudes of different satellites, the difference in the RMS between the results with and without ambiguity resolution is shown. The details are presented in Figure 7.

In Figure 7, the blue and red bars denote the STD of the estimated ISL hardware delay with and without ambiguity resolution, respectively. The green line is the differenced RMS value between the estimated hardware delay with and without ambiguity resolution. We can see that the STD decreases for all satellites except for C38, C40, and C43. The stability of the estimated hardware delay improves by about 10% after ambiguity resolution. In addition to the three IGSO satellites, the STD of the estimated ISL hardware delay is better than 0.05 ns after ambiguity resolution. The RMS of the estimated hardware delay with and without ambiguity resolution performs well in terms of consistency, except for C40, whose difference can reach up to about 0.1 ns. The cause of its formation needs further research.

4.4 Orbit validation

In this section, we assess the quality of orbit determined together with the ISL PCOs and hardware delay estimation from the network solutions. Only satellites in the medium Earth orbit (MEO) for BDS-3 are validated. Considering the public orbit products from IGS are results with ambiguity resolution, we compare our orbit products with ambiguity resolution to the current final orbit products from Wuhan University. The daily difference between two orbit products is counted, and RMS values are obtained. Then, the final RMS values for each MEO satellite can be obtained by averaging the daily RMS values over 14 days of our experiment. The RMS results in along-track, cross-track, radial, and 3D are shown in Figure 8.

We can see that the satellites from C19 to C37 have better accuracy than the satellites from C41 to C46. The RMS values of the former group are about 5.5 cm, 4.0 cm, 3.5 cm, and 8.0 cm in along, cross, radial, and 3D components, respectively. This indicates that accurate orbits are obtained. Obviously there is an increase in the RMS values of satellites from C41 to C46. It almost reaches up to 16.0 cm, 10 cm, 7 cm, and 21 cm in along, cross, radial, and 3D components, respectively. This means that the orbit accuracy of this group of satellites decreases. The detailed statistical RMS values can be seen in Table. 5.

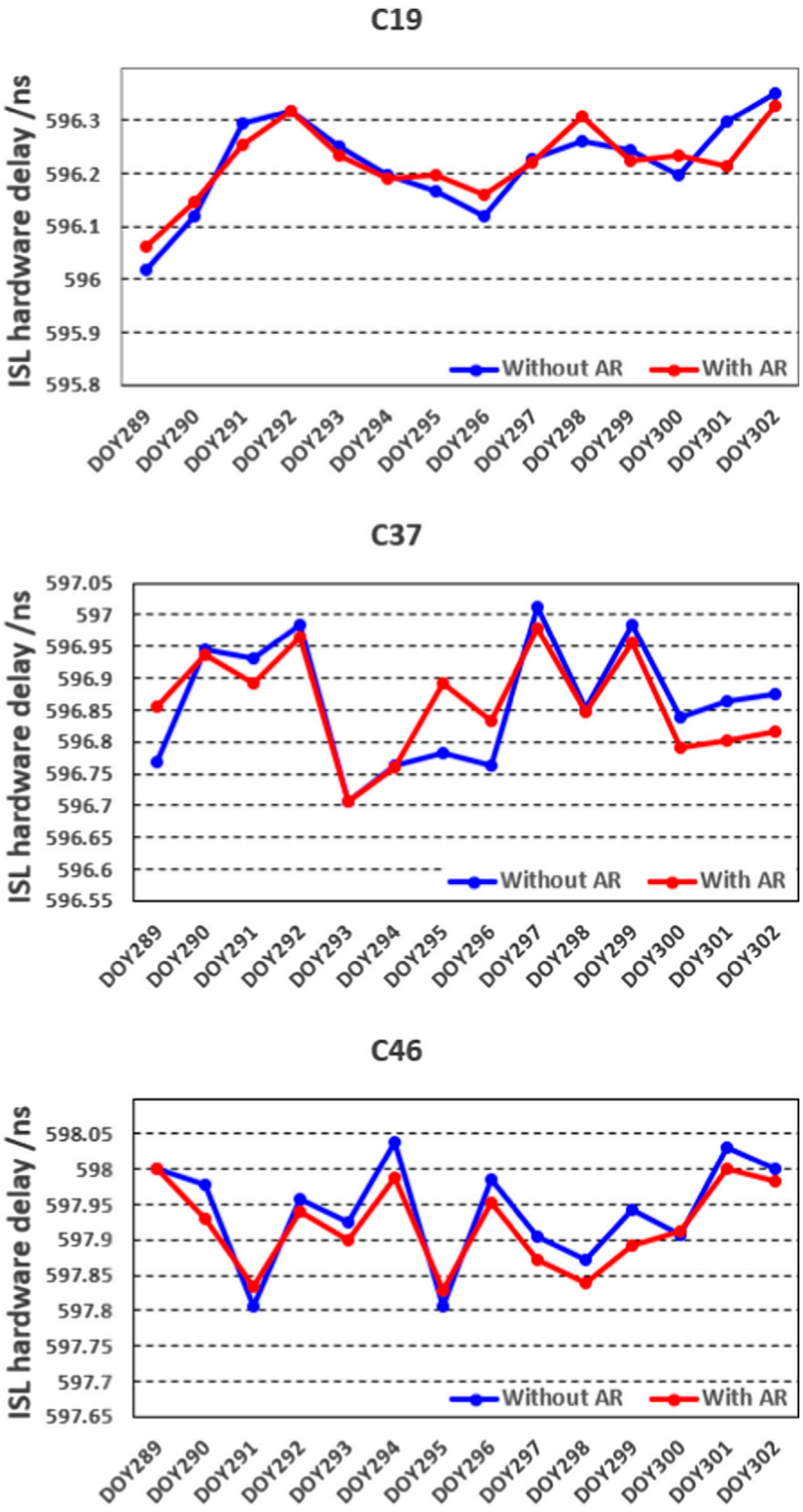

FIGURE 6
Estimated hardware delay in time series during 2 weeks for satellites C19, C37, and C46 as examples.

We conjecture that the different performance of orbit accuracy results from two factors. One is that the product of WHU has not used the ISL observation, but this may not be the major factor because the satellites C19–C37 show good consistency. Another is the number of tracking stations for each satellite. To better understand this phenomenon, the number of stations with tracking ability for every satellite is counted and presented in Figure 9.

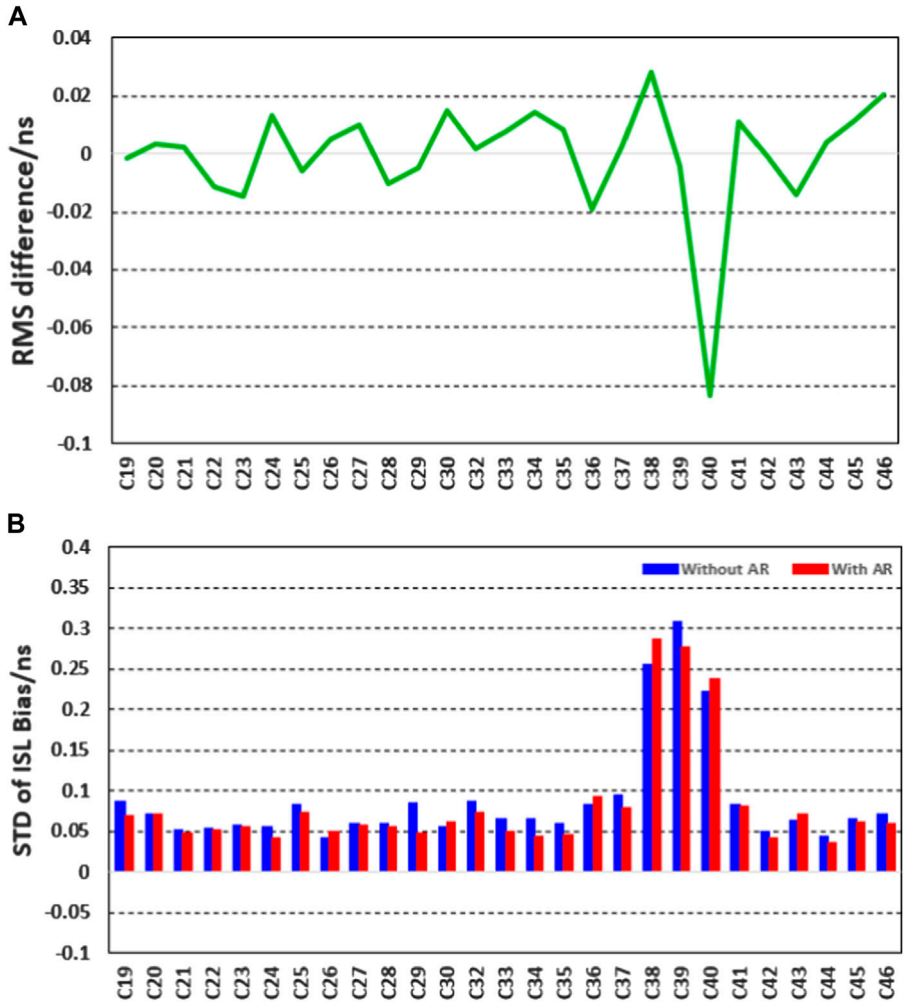

FIGURE 7
Statistical RMS (the upper panel) and STD values (the bottom panel) of ISL hardware delay without ambiguity resolution for all BDS-3 satellites. In **(A)**, the green curve denotes the RMS without ambiguity resolution minus the one with ambiguity resolution; in **(B)**, the blue bars represent the STD without ambiguity while red bars for the one with ambiguity resolution.

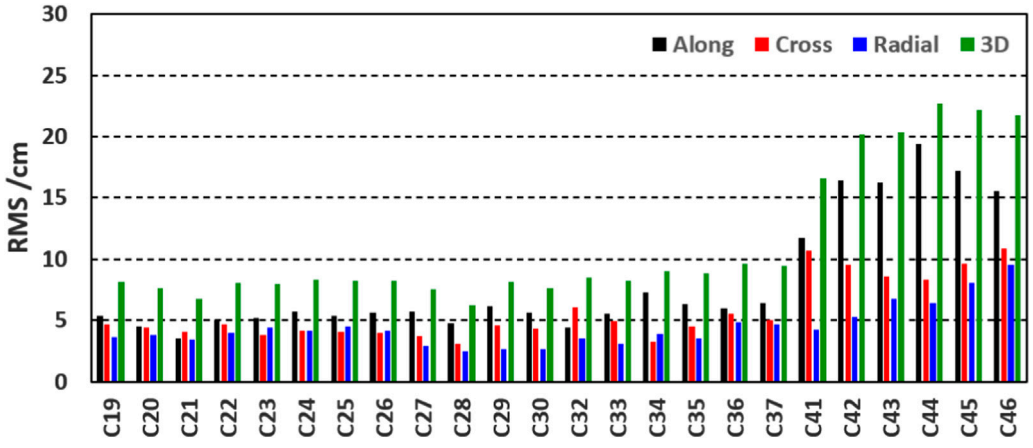

FIGURE 8
Average RMS of each BDS-3 MEO satellite orbit in along-track (the black bars), cross-track (the red bars), radial (the blue bars), and 3D (the green bars) compared to the wum products.

TABLE 5 Statistical RMS values of the BDS-3 MEO satellite orbit.

	Along (cm)	Cross (cm)	Radial (cm)	3D (cm)
RMS average for C19-C37	5.50	4.38	3.70	8.16
RMS average for C41-C46	16.1	9.6	6.7	20.6
RMS average for all MEOs	8.14	5.69	4.46	11.28

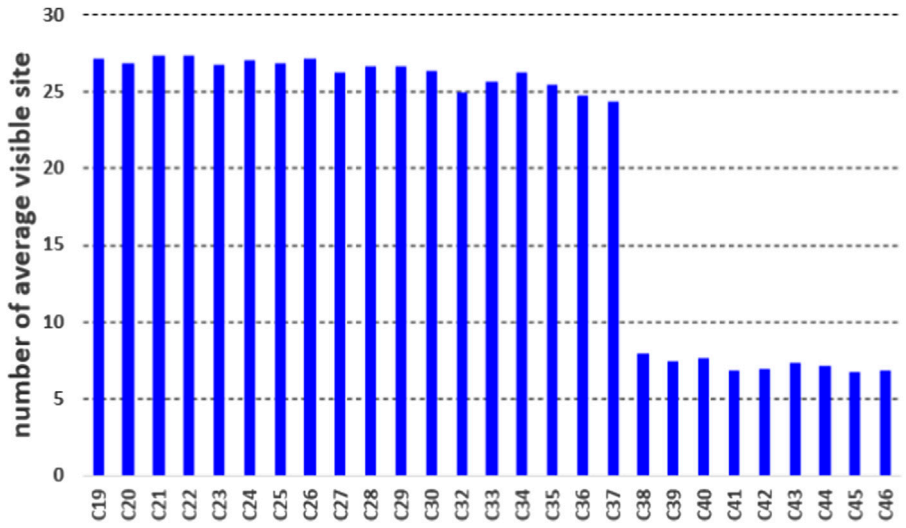

FIGURE 9
Number of average visible stations for every satellite.

According to the previously shown Figure and statistical results, there is an obvious difference in the visible station numbers between the C19–C37 and C41–C46. The average number of the former group is about 25, while it is around 6 for the latter group. In experience, the more the tracking stations and periods are, the better geometrical configuration can be obtained, which contributes to the accuracy of orbit determination. Thus, it is understandable that there is different orbit accuracy for these two groups of satellites. Overall, orbit products produced with the ISL PCOs and hardware delay estimation from network solutions shows good consistency compared with the public final orbit product for the satellites with good configuration. It further validates the effectiveness of the estimated ISL PCOs and hardware delays with ambiguity resolution.

5 Conclusion and discussion

A rapid and successful buildup of the BDS-3 constellation and the realization of ISL technology provide an opportunity for the analysis of orbit and clock, geodesy parameters, and so on. PCOs and hardware delays are two essential factors when using ISL observations. In addition, ambiguity resolution is an essential method for precise data processing. The interrelation of ambiguity resolution and estimation of ISL-related errors has not been explored so far. This contribution focuses on the impact of ambiguity resolution on PCOs and hardware delay estimation of BDS-3 inter-satellite links for the first time.

Also, two weeks of L-band observations from 99 globally distributed ground stations and ISL observations are collected for experimental validation and analysis. First, the effect of introducing ISL observations on ambiguity resolution is investigated. Then, the ISL PCOs and hardware delays estimated using the proposed algorithm with and without ambiguity resolution are obtained and analyzed, respectively. Finally, the estimated orbits in network solutions are assessed to validate the ISL's PCOs and hardware delay estimation. Based on the experimental results, the following conclusions can be summarized:

Introducing ISL observations plays a positive role in ambiguity resolution. The ambiguity fixing rate increases from about 83.5% to 84.5% after introducing ISL observations into L-band observations. Analysis of estimated daily ISL PCOs and hardware delay values shows that there is good consistency for 14 days. Furthermore, the stability of the estimated values improves overall after ambiguity resolution. There is an obvious improvement with proportions of 43%, 27%, and 8% for x-offset, y-offset, and z-offset, respectively. To be specific, different satellites and different components show various improvements. For PCOs, the x-offset and y-offset benefit more from the ambiguity resolution compared to the z-offset for most of the satellites. The average standard deviations of PCO values with ambiguity resolution are 0.012 m, 0.016 m, and 0.032 cm for x-offset, y-offset, and z-offset, respectively. For hardware delays, compared to the ones without ambiguity resolution, STD decreases for all satellites except for C38, C40, and C43. The stability of the estimated hardware delay improves by

about 10% after ambiguity resolution. In addition to the three IGSO satellites, the STD of the estimated ISL hardware delay is better than 0.05 ns The RMS with and without ambiguity resolution performs well in terms of consistency, except for C40. Once the ISL PCOs and hardware delays are well-calibrated with ambiguity resolution, the orbit accuracy is assessed compared to the WUM final products to further validate the estimated ISL PCOs and hardware delays. The daily stability helps ensure stable and accurate orbit products.

The ISL provides a promising way for GNSS orbit determination and clock estimation. The ambiguity resolution when processing L-band and ISL observations in network solutions can have a positive influence on each other. The mechanism needs further investigation.

Data availability statement

The original contributions presented in the study are included in the article/Supplementary Material; further inquiries can be directed to the corresponding author.

Author contributions

ZL performed the theoretical study, conducted the experiment and analysis, and wrote the manuscript; WX revised the manuscript; LF provided conceptualizations and research suggestions; and ZL helped with programming and revised the manuscript. All authors read and agreed to the published version of the manuscript.

Funding

This research was supported in part by the Foundation (U20A0193) and National Natural Science Foundation of China (Grant Nos. 41931075 and 42274041).

Acknowledgments

The authors would like to thank the editors and reviewers for their efforts in supporting the publication of this paper.

Conflict of interest

The authors declare that the research was conducted in the absence of any commercial or financial relationships that could be construed as a potential conflict of interest.

Publisher's note

References

1. Wang H, Xie J, Zhuang J, Wang Z. Performance analysis and progress of inter-satellite-link of Beidou system. In: Proceedings of the 30th International Technical Meeting of the Satellite Division of The Institute of Navigation (ION GNSS+ 2017); September 2017; Portland, OR (2017). p. 1178–85.

2. Rajan JA. Highlights of GPS II-R autonomous navigation. In: Proc. the 58th annual meeting of the Institute of Navigation and CIGTF 21st guidance test symposium; June 24–26; Albuquerque, NM, USA. Institute of Navigation (2002). p. 354–36.

3. Rajan JA, Brodie P, Rawicz H. Modernizing GPS autonomous Navigation with anchor capability. In: Proc. ION GPS/GNSS 2003; September 9–12; Portland, Oregon, USA. Institute of Navigation (2003). p. 1534–42.

4. Tang C, Hu X, Zhou S, Liu L, Pan J, Chen L, et al. Initial results of centralized autonomous orbit determination of the new-generation BDS satellites with inter-satellite link measurements. *J Geodesy* (2018) 92:1155–69. doi:10.1007/s00190-018-1113-7

5. Zhou Y, Wang Y, Huang W, Yang J, Sun L. In-orbit performance assessment of BeiDou intersatellite link ranging. *GPS Solutions* (2018) 22(4):119. doi:10.1007/s10291-018-0784-0

6. Xin X, Tao G, Qile Z, Cai H, Zhang F, Wang X, et al. Precise orbit determination for BDS-3 satellites using satellite-ground and inter-satellite link observations. *GPS Solutions* (2019) 23:40. doi:10.1007/s10291-019-0823-5

7. Xin X, Tao G, Qile Z, Lv Y, Cai H, Liu J. Orbit and clock analysis of BDS-3 satellites using inter-satellite link observations. *J Geodesy* (2020) 94:64. doi:10.1007/s00190-020-01394-4

8. Wang C, Zhao Q, Guo J, Liu J, Chen G. The contribution of intersatellite links to BDS-3 orbit determination: Model refinement and comparisons. *Navigation* (2019) 66: 71–82. doi:10.1002/navi.295

9. Lei G, Fuhong W, Gong X, Sang J, Liu W, Zhang W. Initial results of distributed autonomous orbit determination for Beidou BDS-3 satellites based on inter-satellite link measurements. *GPS Solutions* (2020) 24:72. doi:10.1007/s10291-020-00985-0

10. Ren X, Yang Y, Zhu J, Xu T. Comparing satellite orbit determination by batch processing and extended Kalman filtering using inter-satellite link measurements of the next-generation BeiDou satellites. *GPS Solutions* (2019) 23:25. doi:10.1007/s10291-018-0816-9

11. Ren X, Yang Y, Zhu J, Xu T. Orbit determination of the next generation Beidou satellites with intersatellite link measurements and a priori orbit constraints. *Adv Space Res* (2017) 60(10):2155–65. doi:10.1016/j.asr.2017.08.024

12. Yang D, Yang J, Li G, Zhou Y, Tang C. Globalization highlight: Orbit determination using BeiDou inter-satellite ranging measurements. *GPS Solutions* (2017) 21(3):1395–404. doi:10.1007/s10291-017-0626-5

13. Pan J, Hu X, Zhou S, Tang C, Guo R, Zhu L, et al. Time synchronization of new-generation BDS satellites using inter-satellite link measurements. *Adv Space Res* (2018) 61(1):145–53. doi:10.1016/j.asr.2017.10.004

14. Lou Y, Dai X, Gong X, Li C, Qing Y, Liu Y, et al. A review of real-time multi-GNSS precise orbit determination based on the filter method. *Satellite Navigation* (2022) 3:15. doi:10.1186/s43020-022-00075-1

15. Zhao Q, Guo J, Wang C, Lyu Y, Xu X, Yang C, et al. Precise orbit determination for BDS satellites. *Satellite Navigation* (2022) 3:2. doi:10.1186/s43020-021-00062-y

16. Zuo X, Jiang X, Li P, Wang J, Ge M, Schuh H. A square root information filter for multi-GNSS real-time precise clock estimation. *Satellite Navigation* (2021) 2:28. doi:10.1186/s43020-021-00060-0

17. Li B, Qiao J, Lu Z. Influence of swept-frequency interference on satellite navigation time-domain anti-jamming. *Front Phys* (2022) 10. doi:10.3389/fphy1063474

18. Wu R, Dong J, Wang M. Wearable polarization conversion metasurface MIMO antenna for biomedical applications in 5 GHz WBAN. *Biosensors* (2023) 13(1):73. doi:10.3390/bios13010073

19. Pan Y, Dong J. Design and optimization of an ultrathin and broadband polarization-insensitive fractal FSS using the improved bacteria foraging optimization algorithm and curve fitting. *Nanomaterials* (2023) 13(1):191. doi:10.3390/nano13010191

20. Blewitt G. An automatic editing algorithm for GPS data. *Geophys Res Lett* (1990) 17(3):199–202. Nagivation. Nashville, TN.

21. Ge M, Gendt G, Rothacher M, Shi C, Liu J. Resolution of GPS carrier-phase ambiguities in Precise Point Positioning (PPP) with daily observations. *J Geodesy* (2008) 82:389–99. doi:10.1007/s00190-007-0187-4

22. Laurichesse D, Mercier F. Integer ambiguity resolution on undifferenced GPS phase measurements and its application to PPP. In: Proceedings of the 20th International Technical Meeting of the Satellite Division (2007).

23. Laurichesse D, Mercier F, Berthias JP, Bijac J. Real time zero-difference ambiguities fixing and absolute RTK. In: Proceedings of the 2008 National Technical Meeting of The Institute of Navigation; San Diego, CA (2008).

24. Laurichesse D, Mercier F, Berthias J-P, Broca P, Cerri L. Integer ambiguity resolution on undifferenced GPS phase measurements and its application to PPP and satellite precise orbit determination. *Navig J Inst Navig* (2009) 56(2):135–49. doi:10.1002/j.2161-4296.2009.tb01750.x

25. Geng J, Bock Y. Triple-frequency gps precise point positioning with rapid ambiguity resolution. *J Geodesy* (2013) 87(5):449–60. doi:10.1007/s00190-013-0619-2

26. Geng J, Meng X, Dodson AH, Ge M, Teferle FN. Rapid re-convergences to ambiguity-fixed solutions in precise point positioning. *J Geodesy* (2010) 84:705–14. doi:10.1007/s00190-010-0404-4

27. Geng J, Shi C, Ge M, Dodson AH, Lou Y, Zhao Q, et al. Improving the estimation of fractional-cycle biases for ambiguity resolution in precise point positioning. *J Geodesy* (2012) 86:579–89. doi:10.1007/s00190-011-0537-0

28. Geng J, Teferle FN, Meng X, Dodson AH. Towards PPP-RTK: Ambiguity resolution in real-time precise point positioning. *Adv Space Res* (2011) 47:1664–73. doi:10.1016/j.asr.2010.03.030

29. Gu S, Lou Y, Shi C, Liu J. BeiDou phase bias estimation and its application in precise point positioning with triple-frequency observable. *J Geodesy* (2015) 89:979–92. doi:10.1007/s00190-015-0827-z

30. Wilson BD, Mannucci AJ. Instrumental biases in ionospheric measurement derived from GPS data. In: Proceedings of ION GPS93; September, 1993; Salt Like City (1993). p. 1343–13.

31. Boehm J, Niell A, Tregoning P, Schuh H. Global mapping function (gmf): A new empirical mapping function based on numerical weather model data. *Geophys Res Lett* (2006) 33(7):L07304. doi:10.1029/2005gl025546

32. Schaer S, Steigenberger P. *Determination and use of GPS differential code bias values*. IGS Workshop, https://specialsci.cn/detail/25284480-036c-4588-8a7f-4f05b992f3e7?resourceType=0 (2006).

33. Petit G, Luzum B. *IERS conventions 2010. No. 36 in IERS technical note*. Frankfurt am Main, Germany: Verlag des Bundesamts fürKartographie und Geodäsie (2010).

34. Springer TA, Beutler G, Rothacher M. A new solar radiation pressure model for GPS. *GPS Solutions* (1999) 2(3):673–6. doi:10.1016/s0273-1177(99)00158-1

35. Springer TA, Beutler G, Rothacher M. Improving the orbit estimates of GPS satellites. *J Geodesy* (1999) 73(3):147–57. doi:10.1007/s001900050230

36. Rodriguez-Solano CJ, Hugentobler U, Steigenberger P, Lutz S. Impact of Earth radiation pressure on GPS position estimates. *J Geodesy* (2012) 86(5):309–17. doi:10.1007/s00190-011-0517-4